*Nano Research* 2016, 9(7): 2162–2173
DOI 10.1007/s12274-016-1105-y
**Research Article**

ISSN 1998-0124
CN 11-5974/O4

# Fabrication of sintering-free flexible copper nanowire/polymer composite transparent electrodes with enhanced chemical and mechanical stability

Cho Rong Chu, Changsoo Lee, Jahyun Koo, and Hyuck Mo Lee (✉)

*Department of Materials Science and Engineering, KAIST, 291 Daehak-ro, Yuseong-gu, Daejeon 305-701, Republic of Korea*

**Received:** 15 February 2016
**Revised:** 6 April 2016
**Accepted:** 14 April 2016



**KEYWORDS**
copper nanowires, nanowire/polymer composite, transparent electrode, chemical stability, mechanical stability

## ABSTRACT

The thermal decomposition synthesis of long copper nanowires (CuNWs) was achieved by controlling the synthesis parameters. A detailed study was performed to determine the effect of the molar ratio of copper chloride to nickel acetylacetonate, temperature, and stirring rate on the final shape of the products. Transparent electrodes (TEs) were fabricated by wet treatment with acetic acid (AA), without using a sintering process. The low oxidation stability and high surface roughness are the main disadvantages of the CuNW TEs, which limit their applications. In order to overcome these issues, we prepared CuNW/polymer composite TEs by partial embedding of the CuNWs into poly(methyl methacrylate) (PMMA) on poly(ethylene terephthalate) (PET) substrates. The CuNW/PMMA composite TEs exhibit excellent optoelectronic performance (91.3% at 100.7 Ω/sq), low surface roughness (4.6 nm in height), and good mechanical and chemical stability as compared with CuNW TEs. On the basis of these properties, we believe that CuNW-based composite TEs could serve as low-cost materials for a wide range of new optoelectronic devices.

## 1 Introduction

Transparent electrodes (TEs) are essential components of touch screens, solar cells, liquid crystal displays (LCDs), organic light-emitting diodes (OLEDs), and many other optoelectronic devices [1–4]. Future devices are expected to be capable of bending, stretching, twisting, and deformation into complex and irregular shapes, while maintaining good performance and high reliability. Indium tin oxide (ITO) is widely used in optoelectronic devices because of its high conductivity (~10–30 Ω/sq) and optical transparency (90%). However, ITO is inadequate to satisfy the future requirements of TEs because of the price fluctuation of indium, the brittleness of ITO, and the high temperature used for the fabrication process [1, 5, 6]. These limitations have prompted attempts to develop new alternative materials that are flexible, affordable, and can be deposited at low temperatures. Hence, researchers have attempted to develop alternatives to ITO. Various

Address correspondence to hmlee@kaist.ac.kr

conductive materials, including conducting polymers, carbon nanotubes (CNTs), graphene, and metallic nanowires (NWs), have exhibited encouraging results [7–21]. Among these, metallic NWs are particularly promising. Recent studies have reported the use of metallic NWs, typically silver NWs (AgNWs), for various applications, mainly because of their excellent mechanical, optical, and electronic properties [22–26]. However, the high cost of silver, which is a noble metal, and its limited resources must be accounted for when using AgNWs for the industrial fabrication of optoelectronic devices.

As a result of the increasing demand for low-cost metallic nanowires, copper has received considerable attention as an interesting alternative to silver because it is much more abundant and has a conductivity similar to that of silver. The bulk resistivities of silver and copper are 1.59 nΩ·m and 1.67 nΩ·m, respectively [27]. Thus, various methods for preparing CuNWs, such as chemical vapor deposition, template-assisted electrochemical vapor deposition, and the use of reducing agents, have been reported [28–33]. However, these methods involve complex reaction pathways and require the use of toxic reducing agents, such as hydrazine [19, 20, 33–35]. Wiley and co-workers pioneered the development of CuNW-based TEs and fabricated flexible CuNW TEs exhibiting a sheet resistance of 30 Ω/sq at 85% transmittance [19, 20, 36]. Simonato and co-workers used a glacial acetic acid (AA) solution or poly(3,4-ethylenedioxythiophene):polystyrene sulfonate (PEDOT:PSS) film as a covering layer to clean the CuNWs and then fabricated flexible CuNW TEs with a sheet resistance of 30 Ω/sq at 85% transmittance [34]. However, despite these efforts, CuNW-based TEs still present a number of limitations that prevent their widespread use. One problem is their high surface roughness when deposited on bare substrates, because the large surface fluctuations increase the possibility of electrical short circuits in the resultant devices. Another problem is that vacuum-filtered CuNWs adhere weakly to most substrates (e.g., poly(ethylene terephthalate) (PET), glass, and Si). In addition, CuNWs have low oxidation potential and chemical stability. CuNWs can be easily oxidized under ambient conditions, especially as their diameter decreases. Thus, improving the roughness, adhesion, and stability of CuNW TEs is the key for their application in various electronic devices. An effective strategy to improve the performance of CuNW TEs is the application of a polymeric coating. Gao and co-workers reported the use of a poly(acrylate) matrix to fabricate CuNW composite TEs with a sheet resistance of 220 Ω/sq at 91.5% optical transmittance [37]. Zeng et al. prepared flexible CuNW composite TEs with a sheet resistance of 58.6 Ω/sq at 80% using an elastomer composite [38]. However, most of these CuNW composite TEs have significant drawbacks, such as unstable properties and a higher sheet resistance than CuNW TEs at the same transmittance. Chen et al. [35] prepared CuNW TEs using PEDOT:PSS, with sheet resistances of 760 and 15 Ω/sq and transmittances of 87% and 76%, respectively. Cheng et al. [37] fabricated CuNW/poly(acrylate) composite TEs with transmittances of 91.5% for a 220 Ω/sq sheet resistance, 86.6% for 72 Ω/sq, 80% for 15 Ω/sq, and 70.5% for 5 Ω/sq. Song et al. [38] reported that elastomers composites prepared using CuNW and polydimethylsiloxane (PDMS) and with sheet resistances of 58.6 and 56.4 Ω/sq have transmittances of 80% and 78%, respectively.

Here, we report a synthetic route for the production of thin, ultra-long, and well-dispersed CuNWs. The chemical and mechanical properties of the CuNW-based TEs were improved as follows: (1) by preparing long CuNWs with a small diameter through the control of temperature and stirring rate; (2) by using a vacuum filtration method and an AA treatment to fabricate the CuNW TEs without thermal sintering; and (3) by fabricating the CuNW/polymer composite TEs with the desired surface roughness, chemical stability, and mechanical stability without altering their transmittance and sheet resistance.

## 2 Experimental

### 2.1 Synthesis of CuNWs

CuNWs were synthesized by a two-step non-aqueous method, following a modified reported procedure [28, 38, 39]. First, 1.6 mmol of copper(II) chloride dihydrate ($CuCl_2·H_2O$, Sigma-Aldrich), 0.8 mmol of nickel(II) acetylacetonate ($Ni(acac)_2$, Sigma-Aldrich),

and 20 mL of oleylamine ($C_{18}H_{37}N$, Sigma-Aldrich) were added to a 200 mL two-neck flask, and the mixture was kept under high-purity Ar gas and vigorously stirred at 80 ℃ for 20 min. Next, after complete dissolution of the reagents, the flask was heated at 180 ℃ for 10 h and was then cooled to room temperature. Finally, after centrifugation at 10,000 rpm for 10 min, the obtained CuNWs were washed more than three times with acetone ($CH_3COCH_3$, Samchun Chemical) and hexane ($C_6H_{14}$, <96.0%, Junsei Chemical). A parametric study on the effect of the $CuCl_2{\cdot}2H_2O$:Ni(acac)$_2$ molar ratio (2:1, 1:1, and 1:2), temperature (180, 200, and 220 ℃), and stirring speed (0, 100, and 250 rpm) on the reaction efficiency was performed.

### 2.2 Fabrication of the CuNW/poly(methyl methacrylate) (PMMA) composite TEs

In order to fabricate the NW/polymer composite TEs, the NWs were first dispersed in isopropyl alcohol (IPA) (Dongwoo Fine-Chem.) at a concentration of ~0.02 mg/mL and then filtered through a polytetrafluoroethylene (PTFE) (Sterlitech) membrane. A dilute AA solution (~1 wt.%) was then passed through the membrane to remove organic residues from the surface of the CuNWs. The amount of NW material collected on the filter was controlled so that the resultant coating exhibited different transmittance values. After filtration, the filter membranes were pressed on PET (size: 2.5 cm × 2.5 cm) to transfer the CuNWs and form CuNW TEs. Next, 100 μL of PMMA (495 PMMA A4 resist, MICROCHEM) was coated onto the fabricated CuNW TEs using a spin coater (ACE-200) at 4,000 rpm for 40 s. The CuNW/PMMA composite TEs were then baked on a hot plate at 120 ℃ for 3 min under a $N_2$ atmosphere. Thus, the CuNW/PMMA composite TEs were obtained using forming gases, without thermal sintering.

### 2.3 Characterization

The morphology and dimensions (e.g., diameter and length) of the synthesized CuNWs were investigated by transmission electron microscopy (TEM) (Tecnai TF30 ST, FEI company) and scanning electron microscopy (SEM) (Nova230, FEI company). In order to measure the length and diameter, dilute suspensions of NWs were deposited onto silicon substrates, and SEM and TEM images were acquired. Approximately 50 NWs were analyzed individually, and the average length and diameter were calculated. Moreover, the composition of the CuNWs was assessed by energy-dispersive X-ray spectroscopy (EDS). In order to verify the high purity of the CuNWs, EDS line scanning was performed. The transmittance of the CuNW TE and CuNW/PMMA composite TE was determined using a UV spectrophotometer (UV-3101PC, Shimadzu), and the sheet resistance was measured using a four-point probe station (CMT-SR1000N, Advanced Instrument Technology). In the chemical stability test, the central parts of the CuNW and CuNW/polymer composite TEs were soaked with a drop of an aqueous solution of $Na_2S$ (5 wt.%), and the current was measured by application of a voltage (3 V) using a potentiostat (Interface 1000, GAMRY). The CuNW and CuNW/polymer composite TEs were cut (15 mm × 30 mm) and then subjected to the mechanical and chemical stability tests. The adhesion force was investigated using the 3 M Scotch tape test (No. 522). In the bending test, the CuNW and CuNW/polymer composite TEs were bent in the tensile direction, and the electrical resistance was measured by a multimeter after 100 bending cycles. Moreover, the roughness of the CuNW and CuNW/PMMA composite TEs was determined using a scanning probe microscope (PSIA XE-100, Park Systems).

## 3 Results and discussion

### 3.1 Characterization of CuNWs

We synthesized CuNWs using the thermal decomposition and galvanic displacement methods, which are widely used to prepare, for example, nanoparticles (NPs) and NWs [40, 41]. This process is simple and can produce CuNWs with a higher aspect ratio as compared with other methods. The process can be divided into two steps: a mixing step and a reaction step. The effect of the synthesis conditions, such as the precursor molar ratio, stirring speed, temperature, and injection rate, has been previously investigated for AgNWs. However, few studies have reported the

effect of CuNW synthesis conditions, such as the amount of capping agent, temperature, and stirring speed. In this work, we focused on the effects of temperature and stirring speed, in order to gain further insight into the CuNW synthetic process.

CuNW formation by galvanic displacement and thermal decomposition is well-known. First, during heating, Ni(0) is formed from $Ni^{2+}$ ions in the oleylamine solution. Second, Ni(0) atoms are replaced by $Cu^{2+}$ ions via galvanic displacement; thus, Cu nanostructures appear while Ni(0) disappears, and the catalytic role of $Ni^{2+}$ is complete. Third, the dispersed Cu atoms act as nucleation sites to produce Cu seeds. During this step, the NWs gradually grow. Finally, oleylamine and $Cl^-$ ions can coordinate to metal ions to form CuNWs with a high aspect ratio [28, 39]. Because of their underpotential deposition on the Cu surface, $Ni^{2+}$ ions can also be structure-determining elements. It has been reported that the underpotential deposition of $Ag^+$ ions leads to a predominance of facets with open surface structures, resulting in the one-dimensional growth of Au [42, 43]. Likewise, in this study, initial underpotential deposition of $Ni^{2+}$ ions can occur on the higher energy surface of Cu. Then, the reduced Ni(0) atoms act as a surfactant that reduces the growth rate on the surface, leading to the one-dimensional growth of CuNWs.

The $CuCl_2{\cdot}2H_2O$:$Ni(acac)_2$ molar ratio is an important parameter that determines the morphology of Cu nanostructures. The Cu nanostructures synthesized using different molar ratios of reactants at 180 ℃ are shown in Fig. S1 in the Electronic Supplementary Material (ESM). The Cu nanostructures prepared with a $CuCl_2{\cdot}2H_2O$:$Ni(acac)_2$ molar ratio of 1:2 consist of particles instead of rods or NW structures. As the $CuCl_2{\cdot}2H_2O$:$Ni(acac)_2$ molar ratio increased, CuNWs with a high aspect ratio were formed. The optimum $CuCl_2{\cdot}2H_2O$:$Ni(acac)_2$ molar ratio was determined to be 2:1.

The reaction temperature is another important parameter in the CuNWs synthesis. On the basis of the synthetic process explained above, the $Ni^{2+}$ ions should be preferentially reduced. The CuNWs did not grow at temperatures below 180 ℃, presumably because these temperatures are lower than the thermal decomposition temperature of $Ni(acac)_2$ in oleylamine, which is reported to be 200–220 ℃ [44–46]. Figure 1 and Fig. S2 in the ESM show the SEM and TEM images, respectively, of the CuNWs grown at 180, 200, and 220 ℃ without stirring (0 rpm). As the reaction temperature increased, the CuNWs became thicker and shorter, and the average diameter increased as the temperature increased from 180 to 220 ℃. The average diameter of the NWs ranges from approximately 33.7 to 124.8 nm, depending on the reaction temperature. In addition, the average length of the CuNWs decreased as the reaction temperature increased. The average length of the NWs ranges from approximately 26.7 to 66.9 μm and is dependent on the reaction temperature because the growth of NPs is affected by the reduction rate of the metal ions [47], which is in turn strongly dependent on the reaction temperature. The metal atoms nucleate and grow to form sub-nanometer-sized crystal seeds, followed by nanostructure formation, for which two pathways are considered. In the first pathway, described by Kim et al. during their synthesis of ultra-thin AgNWs using a calix hydroquinone template [48], the seeds grow into anisotropic shapes, such as NWs and rods. This can explain the typical formation of anisotropic particles and the wide diversity of shapes produced in a single reaction medium. In the same study, the metallic face-centered cubic AgNWs were found to grow along the <110> axis. In the second pathway, growth occurs on all crystal faces, and 3D growth leads to the formation of isotropic

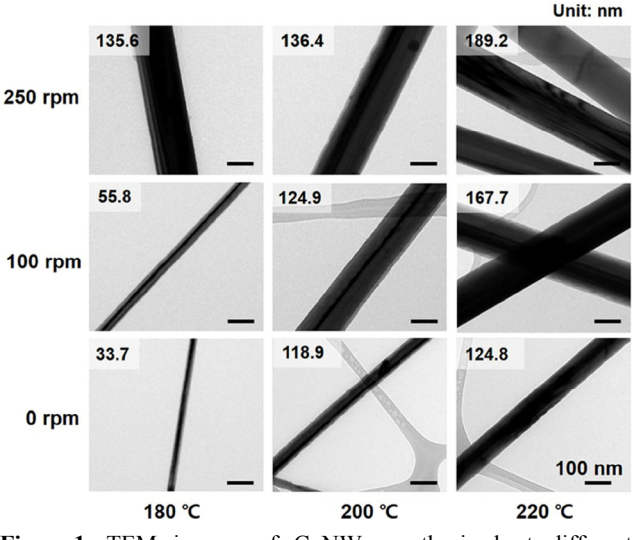


**Figure 1** TEM images of CuNWs synthesized at different stirring rates (0, 100, and 250 rpm) and temperatures (180, 200, and 220 ℃).

particles, such as NPs. Thin NWs were synthesized at a lower temperature, at which the reduction rate of Cu ions is slow, following the first pathway. In contrast, thicker NWs were obtained at higher temperatures, at which the Cu reduction rate is fast, following the second pathway. In addition, differences in length can be attributed to an increased number of nucleation sites at elevated reaction temperatures [49, 50]. The nucleation rate was higher at higher temperatures, resulting in a lower amount of copper precursors per nucleus. Thus, longer NWs were obtained at a lower reaction temperature. These results demonstrate that high aspect ratio CuNWs can be successfully synthesized by controlling the reaction temperature.

The stirring speed of the reaction mixture is also an important parameter in the CuNWs synthesis. Figure 1 and Fig. S2 in the ESM show the SEM and TEM images, respectively, of the CuNWs grown at 180 ˚C with stirring speeds of 0, 100, and 250 rpm. The formation of CuNWs is observed at various stirring speeds, even in stagnant solution. As the stirring speed increased, the CuNWs became thicker and shorter. The average diameter is found to increase as the stirring rate increased from 0 to 250 rpm, and the CuNWs synthesized in the stagnant solution at 180 ˚C have an average diameter of 33.7 nm. In addition, the average length of the CuNWs decreased with increasing stirring speed during the reaction. This result can be explained by the effect of the heating rate on the nucleation rate in the thermal decomposition method. Thus, reaction temperature, heating rate, and solvent type all play an important role in controlling the morphology. The heating rate is a crucial parameter in the synthesis of nanostructures via the thermal decomposition method. Because, as mentioned above, the reduction rate depends strongly on the reaction temperature, and considering that the heating rate of the reaction solution is faster when the stirring speed is high, in mixtures stirred at a high speed the reduction rate is higher as compared with that in solutions with low stirring rates. Thus, isotropic particles, and therefore CuNWs with large diameters, were obtained in mixtures with high stirring speed. This can be explained by the relationship between the aggregation of $Cu^{2+}$ ions, fresh nuclei, and NWs length [50, 51]. Because of the high stirring rates, the $Cu^{2+}$ ions and the fresh nuclei move rapidly and become well dispersed; thus, the new free nuclei can hardly aggregate to form stable, long NWs. In contrast, low stirring speeds, corresponding to low flow velocities, resulted in the aggregation of $Cu^{2+}$ ions and fresh nuclei, thus leading to the formation of stable, long NWs in a mild environment.

Figures 2(a)–2(d) show the TEM image, high-resolution TEM (HRTEM) image, selected area electron diffraction (SAED) pattern, and EDS line scan of the synthesized CuNWs, respectively. The lattice spacing was observed to be 0.21 nm, which corresponds to the (111) plane of fcc Cu. The diffraction patterns indicate that the indexed spots having orientation in the longitudinal direction of the CuNWs are assigned to the growth direction <110> (Fig. 2(c)). In addition, the EDS line scan shows that no Ni component was detected in the CuNWs (Fig. 2(d)), and the X-ray diffraction (XRD) data of the CuNWs synthesized at 180 ˚C and 0 rpm reveal an fcc crystalline structure and very high purity (Fig. S5 in the ESM). Inductively coupled plasma mass spectroscopy (ICP-MS) analysis was carried out to confirm the high purity of the CuNWs prepared at 180 ˚C and 0 rpm. The content of Ni was measured to be only 0.0631 wt.%.

### 3.2 Sintering-free fabrication of CuNW TEs

The vacuum filtration method was successful in coating a wide range of targeted substrates, including glass,

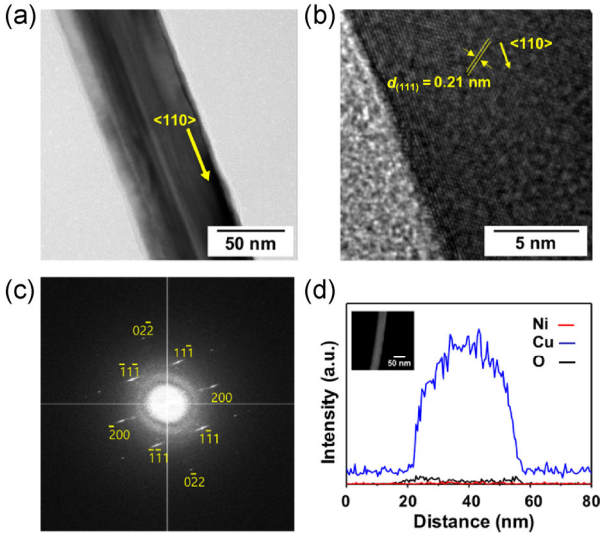


**Figure 2** (a) TEM image, (b) HRTEM image, (c) SAED pattern and (d) EDS line scans of the CuNWs synthesized at 0 rpm (i.e., no stirring) and 180 ˚C.

PET, polyimide (PI), and semiconductor wafers, without surface modification. This method produces TEs with better conductivity as compared with the Meyer rod coating and spray coating techniques, probably because of the higher dispersion of the CuNWs as individual wires. Meyer rod coating can also be used to prepare CuNW TE, but it is not suitable for fabricating stable CuNW inks. Ink formulation includes a number of solvents, such as ethyl acetate, pentyl acetate, 2-propanol, toluene, as well as CuNWs and nitrocellulose as a film former. Owing to the presence of organic materials, such as nitrocellulose, in the CuNWs ink, the CuNW-based TEs have a high sheet resistance. Thus, Meyer rod coating is not suitable for fabricating sintering-free CuNW TEs. In order for the CuNW network to become conductive, the CuNW TEs were thermally sintered in a furnace. However, the thermal sintering temperature (≥180 °C) is too high for transparent plastic or flexible plastic substrates. Thus, a dilute AA solution treatment was adopted to remove residual organic materials without thermal sintering with forming gases. The SEM images in Fig. S3 (in the ESM) show the initial presence of residual organic materials on the substrate and NWs, leading to TEs with a high sheet resistance, and their gradual disappearance as the AA treatment time increased. A treatment of 120 s was required to sufficiently remove the organic components and enhance the contact between the CuNWs. The images show that, even after 120 s of immersion, the CuNWs were not damaged and the electrical properties were almost unchanged.

The transmittance of the TEs is dependent on the amount of CuNWs on the substrates and drastically decreased as the sheet resistance decreased. In addition, the good performance of the CuNW TEs is mainly attributed to geometric features such as long length, small diameter, absence of other NPs, and secure welding. Many studies have addressed the relationship between the size of the CuNWs and the properties of the TEs, such as transmittance and sheet resistance [49, 51, 52]. In this work, transmittance and electrical conductivity are plotted against the NW diameter and length, as shown in Fig. S4 in the ESM. As the stirring speed decreased, the CuNW TEs exhibited higher performance, i.e., higher transmittance at the same resistance and lower sheet resistance at the same transmittance. These results show that high aspect ratio NWs with a small diameter produce a random network with only a few contact points, which corresponds to a lower contact resistance in the TE per unit area as compared with that in TEs with shorter wires. A contact resistance always exists between the wires and it increases as the number of contact points increases. Moreover, small particles result in low transmittance and high sheet resistance. Thus, highly pure CuNWs with high aspect ratio and small diameter are required for the production of high-performance CuNW TEs. On the basis of these results, CuNWs prepared at 180 °C without stirring were selected to fabricate the CuNW-based TEs, in order to achieve the desired aspect ratio and diameter of the CuNWs.

### 3.3 Fabrication of CuNW/PMMA composite electrodes

As mentioned above, CuNW TEs have some disadvantages, including high roughness, weak adhesion, and low chemical stability, which limit their applications. In order to overcome these problems, CuNW/polymer composite TEs were fabricated using PMMA. PMMA has properties, such as low water absorption and chemical stability, which result in better impact strength and environmental stability as compared with polyvinyl alcohol (PVA) and poly(methyl acrylate) (PMA). PMMA is therefore the most suitable material to protect the CuNWs from oxidation. The properties of the CuNW TEs and CuNW/PMMA TEs were compared. Figure 3(a) shows the transmittance graphs and photographs of the CuNW TEs and CuNW/PMMA composite TEs on a PET substrate. The plot of the transmittance versus sheet resistance of CuNW TE and CuNW/PMMA composite TE (Fig. S6 in the ESM) clearly shows that the TE performance was not affected by PMMA coating. In order to analyze the sheet resistance and transmittance, a series of TEs with varying sheet resistances were fabricated by controlling the amount of CuNWs collected during the filtration step. Figure 3(b) shows the transmittance spectra (400–800 nm) of the CuNW/PMMA composite TEs with varying sheet resistance values. At 550 nm, the transmittances are 91.3%, 86.2%, 84.2%, 81.3%, and 67.9% for sheet resistances of 100.7, 35.4, 30.8, 15.8,

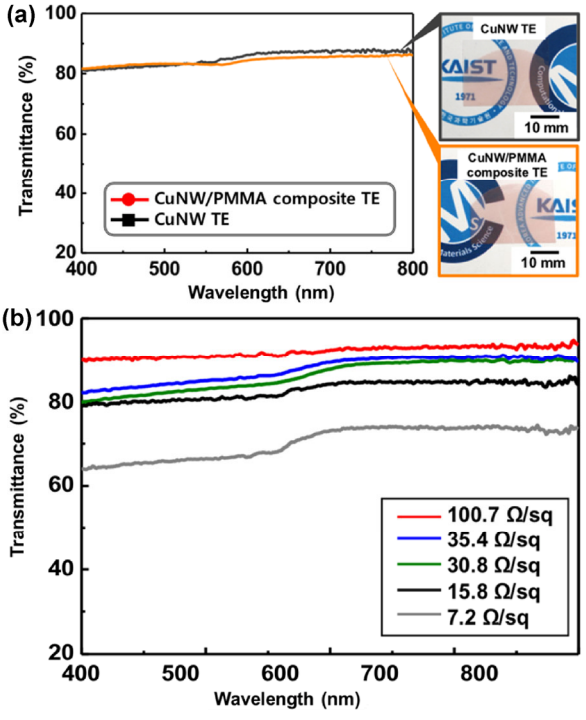


**Figure 3** (a) Transmittance spectra and photographs of the CuNW TE and CuNW/PMMA composite TE and (b) transmittance spectra of the CuNW/PMMA composite TE with various sheet resistances.

and 7.2 Ω/sq, respectively. These results are superior to those reported for other polymer substrate-based TEs [11, 53, 54].

As mentioned before, a large surface height variation is not compatible with various applications and can cause short circuits in electronic devices. Thus, a smooth surface is a critical requirement for the application of TEs to optoelectronic devices. The surface roughness can be reduced by embedding NWs into polymer films. Figure 4 shows the surface topography of a CuNW TE and a CuNW/PMMA composite TE, revealing a dense network of randomly oriented CuNWs. A root-mean-square (RMS) surface roughness of 24.5 nm and a maximum peak-to-valley ($R_{pv}$) height in the range of 131.5 were determined for the CuNW TE (Fig. 4(a)) that has a sheet resistance of 20.5 Ω/sq. On the other hand, the surface topography of the CuNW/polymer composite TE, which has a sheet resistance of 21.0 Ω/sq, appears very smooth (Fig. 4(b)), with RMS surface roughness of 4.6 nm and $R_{pv}$ of 19.1 nm. Clearly, the PMMA coating greatly reduced the surface roughness of the films because the PMMA liquid monomer permeated the CuNW network and filled the holes in the network, including the spaces not occupied by CuNWs on the PET surface.

To confirm the applicability of CuNW/PMMA composite TEs to optoelectronic devices, we successfully fabricated a touch screen panel (TSP) (Fig. S7 in the ESM), which is of a resistive type and has spacers between the upper CuNW/PMMA composite TE and the lower ITO-coated PET substrate. The successful drawing of the word "CMS" on the TSP, as shown in Fig. S7 (in the ESM), shows the promise of CuNW/PMMA composite TEs for use in optoelectronic devices.

### 3.4 Chemical stability

Chemical stability in ambient conditions is another requirement for optoelectronic devices. Despite the many advantages of CuNWs related to cost and conductivity, oxidation stability is still a key issue. Surface oxidation is the main cause of the performance degradation of CuNW TEs, because Cu is much more sensitive than noble metals, such as Ag and Au, to oxygen and moisture in the natural atmosphere. Wiley et al. coated CuNWs with nickel shells, acting as oxidation-resistant layers, by immersing the synthesized CuNWs into $Ni(NO_3)_2$ aqueous solution [52, 55]. Other research groups have also reported the use of core–shell structures to improve the oxidation stability [38, 56, 57]. However, unfortunately, the coating operations increase the processing costs and reduce the performance, e.g., by decreasing the transmittance, of the resultant TEs. The oxidation resistance of CuNW/PMMA composite TEs should be dramatically improved by partial embedding in PMMA. In order to evaluate the oxidation stability, the CuNW and CuNW/PMMA composite TEs were kept under ambient conditions for 30 days. Figure 5 shows the changes in conductivity of the CuNW and CuNW/PMMA composite TEs. The sheet resistance of the CuNW TEs increased rapidly from 6.1 to 21.3 Ω/sq after only 3 days. On the other hand, the CuNW/PMMA composite TEs showed a slow increase in sheet resistance, achieving the same factor of enhancement after 30 days, and the sheet resistance remained very low (25.2 Ω/sq). The oxidation stability was significantly improved after coating with PMMA to form a composite. Thus, the polymer coating effectively protected the CuNWs from moisture and oxygen.

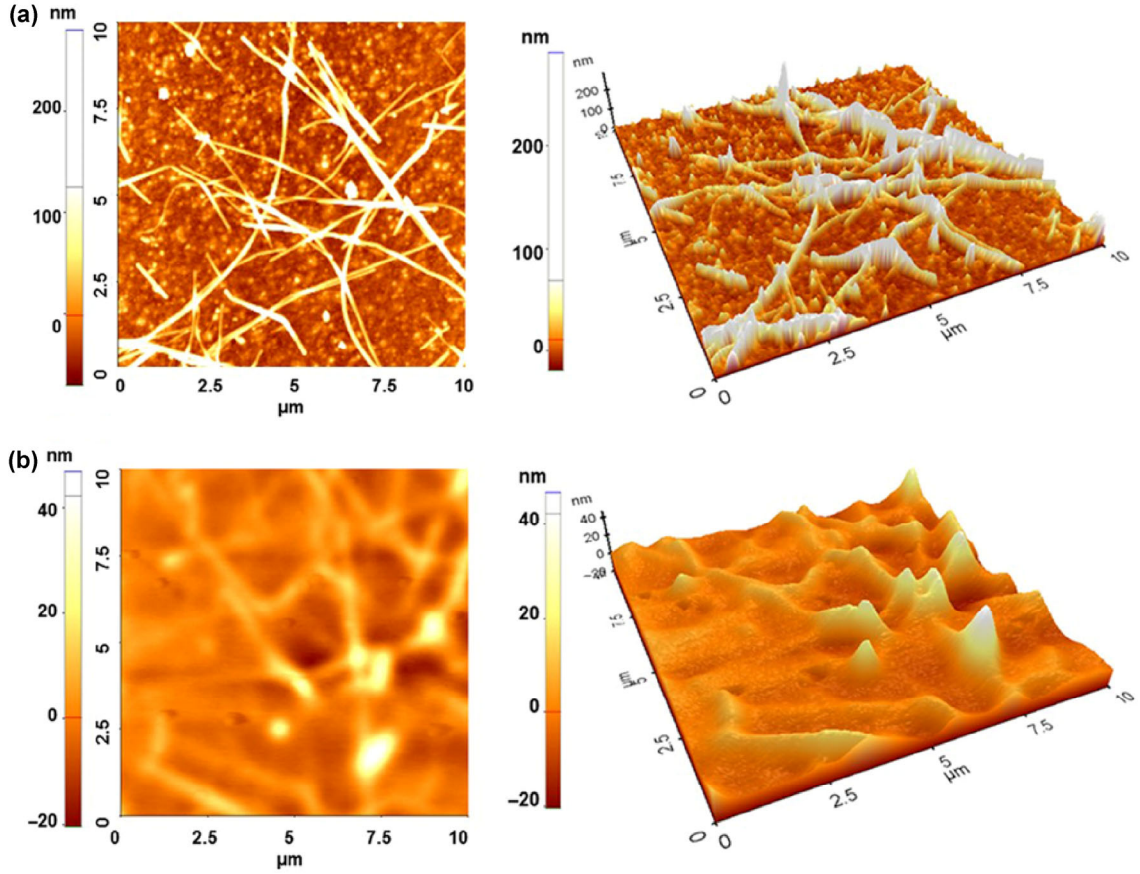


**Figure 4** (a) Atomic force microscopy (AFM) topographic image of the CuNW and (b) AFM topographic image of CuNW/polymer composite TEs.

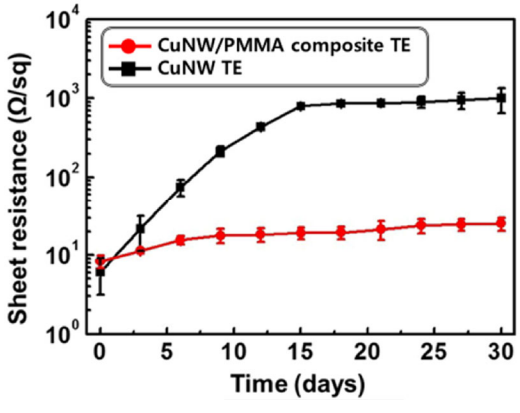


**Figure 5** Change in the sheet resistance of CuNW and CuNW/PMMA composite TEs stored under ambient conditions for 30 days.

We further tested the chemical stability of CuNW/polymer composite TEs (sheet resistance = 27.2 Ω/sq) against corrosive liquids, such as alkali solutions, to evaluate the applicability of these TEs in harsh environments. For this purpose, a drop of a 5 wt.% $Na_2S$ solution was applied to the CuNW-based TEs, as shown in Fig. 6(a). In both cases, the current initially increased (blue area) because of the charged aqueous $Na_2S$ ions. Upon attack of the aqueous $Na_2S$ solution (yellow area), in the unprotected CuNW TEs (black line), the current rapidly decreased because of sulfuration, whereas in the CuNW/polymer composite TEs this drop in current was delayed for more than 60 s. This result can be compared to the clear increase in sheet resistance reported for AgNWs on the surface of PVA, which occurs 59 s after attack by a $Na_2S$ solution [26]. Thus, as shown Fig. 6(b), PMMA protects the NWs from chemical attack, because PMMA is not affected by aqueous solutions of most chemicals, including inorganic acids, alkalis, and aliphatic hydrocarbons.

### 3.5 Mechanical stability

After embedding in PMMA, the CuNW networks

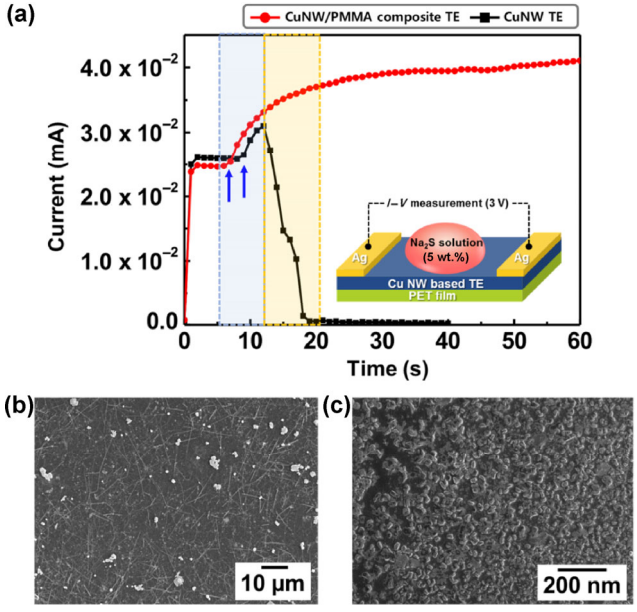


**Figure 6** (a) Changes in the current of CuNW and CuNW/polymer composite TEs over time, upon treatment with aqueous $Na_2S$ solution, (b) SEM image of CuNW TEs after chemical test, and (c) SEM image of CuNW/polymer TEs after chemical test.

become mechanically stable against adhesion, friction, and bending, because all the CuNWs are held tightly together by PMMA. In order to investigate the mechanical stability of the composite TE, a tape test and a friction test were performed. For comparison, CuNW TEs with a similar sheet resistance were also tested. In the tape test, a piece of adhesive tape was attached to the CuNW TE and CuNW/PMMA composite TE, and was then peeled off. For the CuNW TEs, the CuNWs were easily removed from the surface of the PET, and the conductivity was lost (Fig. 7(a)), suggesting that the CuNWs have poor mechanical adhesion to the plastic substrate. On the other hand, for the CuNW/polymer composite TE, the CuNWs were not peeled off (Fig. 7(b)). After this test, the CuNW/polymer composite TE showed no significant increase in sheet resistance. In addition, the CuNW/PMMA composite TE showed no microscopic changes, as shown in Fig. 7(b), and there was no obvious increase in its sheet resistance after wiping with a finger, paper, or cloth.

We further tested the change in electrical resistance when the CuNW-based TEs were bent to a radius of 3.5 mm (Fig. 8). Figure 8 shows the sheet resistance of films after cyclic bending. The variation in sheet

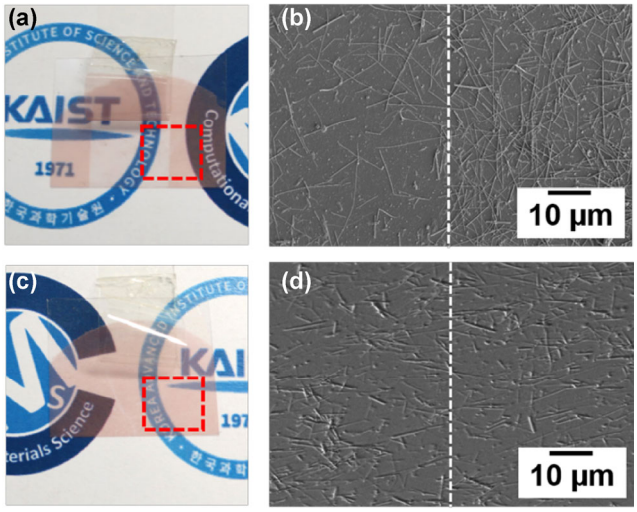


**Figure 7** (a) Photograph and (b) SEM image of CuNW TE before (left) and after (right) adhesion test, and (c) photograph and (d) SEM image of CuNW/PMMA TEs before (left) and after (right) adhesion test.

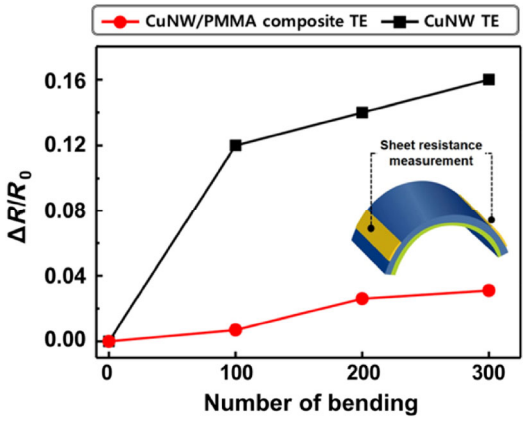


**Figure 8** Plot of $\Delta R/R_0$ versus the number of bending cycles for CuNW and CuNW/polymer TEs after cyclic bending (inset figure: schematic illustration of the bending test).

resistance during the bending test is $\Delta R/R_0$, where $R_0$ is the initial sheet resistance, and $\Delta R$ is the difference between the final and initial sheet resistance values. For the CuNW TE, the variation in sheet resistance increased to 0.16 after 300 cycles of the tensile bending test, as shown in Fig. 8. This is due to the lack of electrical contact between the CuNWs, resulting from their weak adhesion to the substrate. However, for the CuNW/PMMA composite TE, the sheet resistance was not significantly altered even after 300 cycles of the tensile bending test, indicating the superior stability of these TEs against bending deformation as compared with that of the CuNW TE.

## 4 Conclusions

We improved the quality of CuNWs by controlling the synthesis conditions and we demonstrated that sintering-free, flexible CuNW-based TEs with superior chemical and mechanical stability and low surface roughness can be fabricated by partially embedding the CuNWs into a PMMA matrix. The purity of the CuNWs could be controlled by adjusting the precursor molar ratio, synthesis temperature, and stirring rate. The CuNW/PMMA composite TE exhibited a sheet resistance of 100.7 Ω/sq at 91.3% transmittance, which is superior to that of other CuNW-based composite TEs. These TEs show higher chemical stability than CuNW TEs and have good mechanical stability, including high flexibility and strong adhesion. Thus, CuNW-based composite TEs could be used as a low-cost alternative to ITO in various optoelectronic devices, such as OLEDs and solar cells. We believe that this work represents an important advance toward the application of CuNW-based TEs in flexible optoelectronic applications.

## Acknowledgments

This research was supported by a National Research Foundation (NRF) of Korea grant funded by the Korean government (MEST) (No. 2011-0028612) and an NRF of Korea grant funded by the Korean Government (MSIP) (No. NRF-2015R1A5A1037627).

**Electronic supplementary Material:** Supplementary material (Cu nanostructures with different molar ratios, graph of diameters and lengths of CuNWs, evolution of sheet resistance and transmittance of the CuNW TEs using CuNWs with different aspect ratios) is available in the online version of this article at http://dx.doi.org/10.1007/s12274-016-1105-y.

## References

[1] Gordon, R. G. Criteria for choosing transparent conductors. *MRS Bull.* **2000**, *25*, 52–57.

[2] Gaynor, W.; Lee, J.-Y.; Peumans, P. Fully solution-processed inverted polymer solar cells with laminated nanowire electrodes. *ACS Nano* **2010**, *4*, 30–34.

[3] Madaria, A. R.; Kumar, A.; Zhou, C. W. Large scale, highly conductive and patterned transparent films of silver nanowires on arbitrary substrates and their application in touch screens. *Nanotechnology* **2011**, *22*, 245201.

[4] Van De Lagemaat, J.; Barnes, T. M.; Rumbles, G.; Shaheen, S. E.; Coutts, T. J.; Weeks, C.; Levitsky, I.; Peltola, J.; Glatkowski, P. Organic solar cells with carbon nanotubes replacing $In_2O_3$: Sn as the transparent electrode. *Appl. Phys. Lett.* **2006**, *88*, 233503.

[5] Leterrier, Y.; Médico, L.; Demarco, F.; Månson, J.-A. E.; Betz, U.; Escola, M. F.; Olsson, M. K.; Atamny, F. Mechanical integrity of transparent conductive oxide films for flexible polymer-based displays. *Thin Solid Films* **2004**, *460*, 156–166.

[6] Minami, T. Transparent conducting oxide semiconductors for transparent electrodes. *Semicond. Sci. Technol.* **2005**, *20*, S35.

[7] Hecht, D. S.; Hu, L. B.; Irvin, G. Emerging transparent electrodes based on thin films of carbon nanotubes, graphene, and metallic nanostructures. *Adv. Mater.* **2011**, *23*, 1482–1513.

[8] Hong, W. J.; Xu, Y. X.; Lu, G. W.; Li, C.; Shi, G. Q. Transparent graphene/PEDOT–PSS composite films as counter electrodes of dye-sensitized solar cells. *Electrochem. Commun.* **2008**, *10*, 1555–1558.

[9] Doherty, E. M.; De, S.; Lyons, P. E.; Shmeliov, A.; Nirmalraj, P. N.; Scardaci, V.; Joimel, J.; Blau, W. J.; Boland, J. J.; Coleman, J. N. The spatial uniformity and electromechanical stability of transparent, conductive films of single walled nanotubes. *Carbon* **2009**, *47*, 2466–2473.

[10] Hu, L.; Hecht, D. S.; Grüner, G. Percolation in transparent and conducting carbon nanotube networks. *Nano Lett.* **2004**, *4*, 2513–2517.

[11] Tung, V. C.; Chen, L.-M.; Allen, M. J.; Wassei, J. K.; Nelson, K.; Kaner, R. B.; Yang, Y. Low-temperature solution processing of graphene−carbon nanotube hybrid materials for high-performance transparent conductors. *Nano Lett.* **2009**, *9*, 1949–1955.

[12] Azulai, D.; Belenkova, T.; Gilon, H.; Barkay, Z.; Markovich, G. Transparent metal nanowire thin films prepared in mesostructured templates. *Nano Lett.* **2009**, *9*, 4246–4249.

[13] Wu, H.; Hu, L. B.; Rowell, M. W.; Kong, D. S.; Cha, J. J.; McDonough, J. R.; Zhu, J.; Yang, Y.; McGehee, M. D.; Cui, Y. Electrospun metal nanofiber webs as high-performance transparent electrode. *Nano Lett.* **2010**, *10*, 4242–4248.

[14] Leem, D. S.; Edwards, A.; Faist, M.; Nelson, J.; Bradley, D. D. C.; de Mello, J. C. Efficient organic solar cells with solution-processed silver nanowire electrodes. *Adv. Mater.* **2011**, *23*, 4371–4375.

[15] Hu, L. B.; Kim, H. S.; Lee, J.-Y.; Peumans, P.; Cui, Y. Scalable coating and properties of transparent, flexible, silver nanowire electrodes. *ACS Nano* **2010**, *4*, 2955–2963.

[16] Scardaci, V.; Coull, R.; Lyons, P. E.; Rickard, D.; Coleman, J. N. Spray deposition of highly transparent, low-resistance networks of silver nanowires over large areas. *Small* **2011**, *7*, 2621–2628.

[17] Won, Y.; Kim, A.; Lee, D.; Yang, W.; Woo, K.; Jeong, S.; Moon, J. Annealing-free fabrication of highly oxidation-resistive copper nanowire composite conductors for photovoltaics. *NPG Asia Mater.* **2014**, *6*, e105.

[18] Guo, H. Z.; Lin, N.; Chen, Y. Z.; Wang, Z. W.; Xie, Q. S.; Zheng, T. C.; Gao, N.; Li, S. P.; Kang, J.; Cai, D. J. et al. Copper nanowires as fully transparent conductive electrodes. *Sci. Rep.* **2013**, *3*, 2323.

[19] Rathmell, A. R.; Wiley, B. J. The synthesis and coating of long, thin copper nanowires to make flexible, transparent conducting films on plastic substrates. *Adv. Mater.* **2011**, *23*, 4798–4803.

[20] Rathmell, A. R.; Bergin, S. M.; Hua, Y. L.; Li, Z. Y.; Wiley, B. J. The growth mechanism of copper nanowires and their properties in flexible, transparent conducting films. *Adv. Mater.* **2010**, *22*, 3558–3563.

[21] Lee, J.; Lee, I.; Kim, T. S.; Lee, J. Y. Efficient welding of silver nanowire networks without post-processing. *Small* **2013**, *9*, 2887–2894.

[22] Celle, C.; Mayousse, C.; Moreau, E.; Basti, H.; Carella, A.; Simonato, J.-P. Highly flexible transparent film heaters based on random networks of silver nanowires. *Nano Res.* **2012**, *5*, 427–433.

[23] Mayousse, C.; Celle, C.; Moreau, E.; Mainguet, J.-F.; Carella, A.; Simonato, J.-P. Improvements in purification of silver nanowires by decantation and fabrication of flexible transparent electrodes. Application to capacitive touch sensors. *Nanotechnology* **2013**, *24*, 215501.

[24] Coskun, S.; Selen Ates, E.; Unalan, H. E. Optimization of silver nanowire networks for polymer light emitting diode electrodes. *Nanotechnology* **2013**, *24*, 125202.

[25] Gaynor, W.; Burkhard, G. F.; McGehee, M. D.; Peumans, P. Smooth nanowire/polymer composite transparent electrodes. *Adv. Mater.* **2011**, *23*, 2905–2910.

[26] Zeng, X. Y.; Zhang, Q. K.; Yu, R. M.; Lu, C. Z. A new transparent conductor: Silver nanowire film buried at the surface of a transparent polymer. *Adv. Mater.* **2010**, *22*, 4484–4488.

[27] Hu, L. B.; Wu, H.; Cui, Y. Metal nanogrids, nanowires, and nanofibers for transparent electrodes. *MRS Bull.* **2011**, *36*, 760–765.

[28] Guo, H. Z.; Lin, N.; Chen, Y. Z.; Wang, Z. W.; Xie, Q. S.; Zheng, T. C.; Gao, N.; Li, S. P.; Kang, J.; Cai, D. J. et al. Copper nanowires as fully transparent conductive electrodes. *Sci. Rep.* **2013**, *3*, 2323.

[29] Choi, H.; Park, S.-H. Seedless growth of free-standing copper nanowires by chemical vapor deposition. *J. Am. Chem. Soc.* **2004**, *126*, 6248–6249.

[30] Zhao, Y. X.; Zhang, Y.; Li, Y. P.; Yan, Z. F. Soft synthesis of single-crystal copper nanowires of various scales. *New J. Chem.* **2012**, *36*, 130–138.

[31] Gao, T.; Meng, G. W.; Wang, Y. W.; Sun, S. H.; Zhang, L. D. Electrochemical synthesis of copper nanowires. *J. Phys.: Condens. Matter* **2002**, *14*, 355.

[32] Molares, M. T.; Buschmann, V.; Dobrev, D.; Neumann, R.; Scholz, R.; Schuchert, I. U.; Vetter, J. Single-crystalline copper nanowires produced by electrochemical deposition in polymeric ion track membranes. *Adv. Mater.* **2001**, *13*, 62–65.

[33] Chang, Y.; Lye, M. L.; Zeng, H. C. Large-scale synthesis of high-quality ultralong copper nanowires. *Langmuir* **2005**, *21*, 3746–3748.

[34] Mayousse, C.; Celle, C.; Carella, A.; Simonato, J.-P. Synthesis and purification of long copper nanowires. Application to high performance flexible transparent electrodes with and without PEDOT:PSS. *Nano Res.* **2014**, *7*, 315–324.

[35] Chen, J. Y.; Zhou, W. X.; Chen, J.; Fan, Y.; Zhang, Z. Q.; Huang, Z. D.; Feng, X. M.; Mi, B. X.; Ma, Y. W.; Huang, W. Solution-processed copper nanowire flexible transparent electrodes with PEDOT: PSS as binder, protector and oxide-layer scavenger for polymer solar cells. *Nano Res.* **2015**, *8*, 1017–1025.

[36] Ye, S. R.; Rathmell, A. R.; Stewart, I. E.; Ha, Y. C.; Wilson, A. R.; Chen, Z. F.; Wiley, B. J. A rapid synthesis of high aspect ratio copper nanowires for high-performance transparent conducting films. *Chem. Commun.* **2014**, *50*, 2562–2564.

[37] Cheng, Y.; Wang, S. L.; Wang, R. R.; Sun, J.; Gao, L. Copper nanowire based transparent conductive films with high stability and superior stretchability. *J. Mater. Chem. C* **2014**, *2*, 5309–5316.

[38] Song, J. Z.; Li, J. H.; Xu, J. Y.; Zeng, H. B. Superstable transparent conductive Cu@$Cu_4Ni$ nanowire elastomer composites against oxidation, bending, stretching, and twisting for flexible and stretchable optoelectronics. *Nano Lett.* **2014**, *14*, 6298–6305.

[39] Guo, H. Z.; Chen, Y. Z.; Ping, H. M.; Jin, J. R.; Peng, D.-L. Facile synthesis of Cu and Cu@Cu–Ni nanocubes and nanowires in hydrophobic solution in the presence of nickel and chloride ions. *Nanoscale* **2013**, *5*, 2394–2402.

[40] Lee, C.; Kim, N. R.; Koo, J.; Lee, Y. J.; Lee, H. M. Cu-Ag core–shell nanoparticles with enhanced oxidation stability for printed electronics. *Nanotechnology* **2015**, *26*, 455601.

[41] Kim, N. R.; Shin, K.; Jung, I.; Shim, M.; Lee, H. M. Ag–Cu bimetallic nanoparticles with enhanced resistance to oxidation:

A combined experimental and theoretical study. *J. Phys. Chem. C* **2014**, *118*, 26324–26331.

[42] Personick, M. L.; Langille, M. R.; Zhang, J.; Mirkin, C. A. Shape control of gold nanoparticles by silver underpotential deposition. *Nano Lett.* **2011**, *11*, 3394–3398.

[43] Liu, M. Z.; Guyot-Sionnest, P. Mechanism of silver(I)-assisted growth of gold nanorods and bipyramids. *J. Phys. Chem. B* **2005**, *109*, 22192–22200.

[44] Carenco, S.; Boissière, C.; Nicole, L.; Sanchez, C.; Le Floch, P.; Mézailles, N. Controlled design of size-tunable monodisperse nickel nanoparticles. *Chem. Mater.* **2010**, *22*, 1340–1349.

[45] Li, Y.; Afzaal, M.; O'Brien, P. The synthesis of amine-capped magnetic (Fe, Mn, Co, Ni) oxide nanocrystals and their surface modification for aqueous dispersibility. *J. Mater. Chem.* **2006**, *16*, 2175–2180.

[46] van Embden, J.; Chesman, A. S. R.; Jasieniak, J. J. The heat-up synthesis of colloidal nanocrystals. *Chem. Mater.* **2015**, *27*, 2246–2285.

[47] Bhatt, A. I.; Mechler, Á.; Martin, L. L.; Bond, A. M. Synthesis of Ag and Au nanostructures in an ionic liquid: Thermodynamic and kinetic effects underlying nanoparticle, cluster and nanowire formation. *J. Mater. Chem.* **2007**, *17*, 2241–2250.

[48] Hong, B. H.; Bae, S. C.; Lee, C.-W.; Jeong, S.; Kim, K. S. Ultrathin single-crystalline silver nanowire arrays formed in an ambient solution phase. *Science* **2001**, *294*, 348–351.

[49] Bergin, S. M.; Chen, Y. H.; Rathmell, A. R.; Charbonneau, P.; Li, Z. Y.; Wiley, B. J. The effect of nanowire length and diameter on the properties of transparent, conducting nanowire films. *Nanoscale* **2012**, *4*, 1996–2004.

[50] Araki, T.; Jiu, J. T.; Nogi, M.; Koga, H.; Nagao, S.; Sugahara, T.; Suganuma, K. Low haze transparent electrodes and highly conducting air dried films with ultra-long silver nanowires synthesized by one-step polyol method. *Nano Res.* **2014**, *7*, 236–245.

[51] Jiu, J.; Araki, T.; Wang, J.; Nogi, M.; Sugahara, T.; Nagao, S.; Koga, H.; Suganuma, K.; Nakazawa, E.; Hara, M. et al. Facile synthesis of very-long silver nanowires for transparent electrodes. *J. Mater. Chem. A* **2014**, *2*, 6326–6330.

[52] Rathmell, A. R.; Nguyen, M.; Chi, M. F.; Wiley, B. J. Synthesis of oxidation-resistant cupronickel nanowires for transparent conducting nanowire networks. *Nano Lett.* **2012**, *12*, 3193–3199.

[53] Yu, Z. B.; Niu, X. F.; Liu, Z. T.; Pei, Q. B. Intrinsically stretchable polymer light-emitting devices using carbon nanotube-polymer composite electrodes. *Adv. Mater.* **2011**, *23*, 3989–3994.

[54] De, S.; Lyons, P. E.; Sorel, S.; Doherty, E. M.; King, P. J.; Blau, W. J.; Nirmalraj, P. N.; Boland, J. J.; Scardaci, V.; Joimel, J. et al. Transparent, flexible, and highly conductive thin films based on polymer−nanotube composites. *ACS Nano* **2009**, *3*, 714–720.

[55] Stewart, I. E.; Rathmell, A. R.; Yan, L.; Ye, S. R.; Flowers, P. F.; You, W.; Wiley, B. J. Solution-processed copper–nickel nanowire anodes for organic solar cells. *Nanoscale* **2014**, *6*, 5980–5988.

[56] Stewart, I. E.; Ye, S. R.; Chen, Z. F.; Flowers, P. F.; Wiley, B. J. Synthesis of Cu–Ag, Cu–Au, and Cu–Pt core–shell nanowires and their use in transparent conducting films. *Chem. Mater.* **2015**, *27*, 7788–7794.

[57] Chen, J. Y.; Chen, J.; Li, Y.; Zhou, W. X.; Feng, X. M.; Huang, Q. L.; Zheng, J. G.; Liu, R. Q.; Ma, Y. W.; Huang, W. Enhanced oxidation-resistant Cu-Ni core–shell nanowires: Controllable one-pot synthesis and solution processing to transparent flexible heaters. *Nanoscale* **2015**, *7*, 16874–16879.